

Article

Effects of Ni-Ti Content on Mechanical Properties of Laser Cladding A100-(Ni-Ti) Coatings

Tengfei Han ^{1,2,*} , Xinyu Yao ¹, Xusheng Mao ¹, Bo Wen ¹, Penghui Liang ¹, Tangya Yan ¹ and Xinghui Zhu ^{3,*}

¹ College of Mechanical Engineering, Nanjing Vocational University of Industry Technology (NJUIT), Nanjing 210023, China; yao13016850682@outlook.com (X.Y.); 13605216878@163.com (X.M.); a15912549856@163.com (B.W.); 13419397880@163.com (P.L.); 13382933639@163.com (T.Y.)

² Industrial Perception and Intelligent Manufacturing Equipment Engineering Research Center of Jiangsu Province, Nanjing Vocational University of Industry Technology, Nanjing 210023, China

³ China Special Equipment Inspection & Research Institute, Beijing 100029, China

* Correspondence: tfhan2021@foxmail.com (T.H.); zhuxinghui1@126.com (X.Z.)

Abstract: Among many methods to enhance the crack resistance of laser cladding coatings, adjusting the composition of laser cladding material is the most simple, feasible, and effective method. To improve the plastic toughness and crack resistance of A100 laser cladding coating, Ni and Ti powders of an equal molar ratio were added to A100 powder as laser cladding powder. Laser cladding technology prepared A100-(Ni-Ti) coatings without crack defects. The cladding coatings' phase composition and microstructure were analyzed using XRD and SEM, respectively. A ring-block friction and wear tester tested the wear resistance of the A100-(Ni-Ti) cladding coatings. A100-(Ni-Ti) cladding coatings mainly contain martensite and austenite. The elements Ni and Ti are distributed primarily in the austenitic phase region. The results show that adding Ni and Ti elements can reduce the microhardness of A100 cladding coatings. The average microhardness of the A100-0%(Ni-Ti) cladding coating is 532.50 HV, and the average microhardness of the A100-10%(Ni-Ti) cladding coating is 430.99 HV, while the average microhardness of the A100-30%(Ni-Ti) cladding coating is only 307.49 HV. The wear surface of the A100-10%(Ni-Ti) cladding mainly shows pits and a small amount of adhesive wear. The A100-20%(Ni-Ti) and A100-30%(Ni-Ti) cladding coatings show severe adhesive wear. The A100-10%(Ni-Ti) cladding with high microhardness and good run-in performance exhibits the best wear resistance.

Keywords: laser cladding; A100-(Ni-Ti); microstructure; microhardness; wear resistance



Academic Editor: Raul Arrabal

Received: 17 December 2024

Revised: 27 January 2025

Accepted: 30 January 2025

Published: 2 February 2025

Citation: Han, T.; Yao, X.; Mao, X.; Wen, B.; Liang, P.; Yan, T.; Zhu, X. Effects of Ni-Ti Content on Mechanical Properties of Laser Cladding A100-(Ni-Ti) Coatings. *Coatings* **2025**, *15*, 160. <https://doi.org/10.3390/coatings15020160>

Copyright: © 2025 by the authors. Licensee MDPI, Basel, Switzerland. This article is an open access article distributed under the terms and conditions of the Creative Commons Attribution (CC BY) license (<https://creativecommons.org/licenses/by/4.0/>).

1. Introduction

With the progress of technology and the development of social productivity, the reliability of machinery and equipment is increasingly required. During the operation of mechanical equipment, friction and wear are inevitable, and the wear resistance of parts (especially gears, shafts, etc.) directly affects the accuracy, work efficiency and service life of mechanical equipment. Therefore, improving the wear resistance of mechanical parts is an important measure to ensure the long-term stable operation of mechanical equipment, reduce the failure rate, and improve work efficiency.

Different from the formation mechanisms of cracks and fatigue fracture, wear begins on the surface of parts [1]. Hence, improving the wear resistance of the surface of parts is an effective way to prolong their service life. Among many surface modification technologies, laser cladding has been widely studied and applied in engineering because of its advantages, such as its small heat-affected zone, dense structure, high efficiency, low

energy consumption, and low pollution [2,3]. In addition, laser cladding technology has a high utilization rate for cladding materials, greatly reducing the manufacturing cost of cladding coatings. Because of this, laser cladding processes have become a desired way to increase the surface properties of parts [4,5]. In the process of the rapid melting and solidification of laser cladding, it is easy for the cladding coatings to have huge residual stress [6], which easily increases the tendency of the cladding coatings to crack or directly cause the cladding coatings to crack. Once the surface of the cladding coating cracks, it will significantly reduce the effect of improving the surface performance of the cladding coating. Therefore, it is necessary to avoid cracks in cladding coatings in the preparation process of laser cladding coatings.

To avoid the appearance of cracks in the laser cladding process, the cracks' causes must be analyzed first. The mechanism of macroscopic crack formation in cladding is that the strain caused by stress tensile generated in cladding is greater than the plastic strain capacity of the cladding coatings itself, resulting in cracking [7]. The cladding coating's pores, inclusions, and internal micro-cracks are the crack source or extension path. During the growth of the eutectic structure of laser cladding coating and the thick dendrites at the bottom of the cladding coating, due to the existence of dendrite segregation, intergranular weakening is caused, and cracks often propagate along their grain boundaries. It can be observed that the cracks of cladding coatings are brittle fractures, and the stress caused by cracks are mainly three kinds: residual stress, thermal stress, and microstructural stress. According to the mechanism of laser cladding coating cracks, the prevention and control measures primarily include optimizing the composition of cladding powder, optimizing the parameters of laser cladding, the heat treatment of materials, and increasing the auxiliary physical field.

1. Optimize the design of the cladding powder composition

Due to the difference in physical properties between the matrix and the cladding coating, the coating will produce sizeable residual stress after processing. The magnitude of thermal stress with different expansion coefficients can be expressed by Formula (1) [8].

$$\sigma = \frac{(\alpha_1 - \alpha_2)\Delta TE}{1 - \lambda} \quad (1)$$

where σ is thermal stress; α_2 is the thermal expansion coefficient of cladding coating; α_1 is the thermal expansion coefficient of the substrate; ΔT is the temperature difference between the cladding coating and the room temperature; E is the elastic modulus of the cladding coating; and λ is the Poisson ratio of the cladding coating.

It can be seen from Formula (1) that reducing the difference between the thermal expansion coefficient of the cladding coating and the substrate can reduce the thermal stress. To reduce the stress, the thermal expansion coefficient of the cladding coating can be made similar to that of the substrate by changing the powder composition to reduce the tendency of minor cracking, or the toughness of the cladding coating can be increased to prevent it from cracking easily under the action of stress. In addition, adding large particles with high melting points, such as ceramics, can refine the grain and reduce the structural stress caused by element segregation.

Xuehui Shen et al. [9] studied the effect of WC content on the crack behavior of laser-cladding metal–ceramic composite coatings. The research results show that the composite coating had no cracks when the WC content was 40%, while the composite coating had cracks when the WC content was 50% and 60%. The addition of WC in the composite coating increased from 40% to 50% and 60%, and the microhardness of the composite coating increased by only 3%. In comparison, the tensile stress of the composite coating increased by 10.3%, which significantly increased the probability of cracks in the composite

coating. Zhenwei Li et al.'s [10] laser cladding preparation of WC-reinforced Ni50A coatings found that the coatings will produce cracks and pores. They added Ti element with different content to the coatings and investigated the effect of Ti element on the crack. The results show that the Ti element can eliminate the cracks in the coating. Ti element can prolong the existence time of the molten pool and disperse the stress concentration between the precipitated phase of the coating and the substrate phase. In addition, the in-situ synthesis of TiC/TiWC₂ results in bulk precipitates in the coating. These improve the cracking and porosity of the WC-Ni50A coating. Mingke Li et al. [11] researched the mechanism of improving the crack resistance, microstructure, and properties of laser cladding WC-Ni60AA coating by Mo element. When Mo element is not added to the coating, there are more cracks. When one wt%Mo element is added, cracks in the coating are entirely eliminated. However, when the amount of Mo element added increases or decreases, the coating will have cracks. The existing research results show that the coating cracks can be effectively reduced or eliminated by adjusting the composition of cladding materials.

2. Optimization of laser cladding parameters

Process parameters that can usually be adjusted include laser power, spot diameter, cladding coating thickness, powder feeding mode, cladding speed, and protective gas flow. These parameters affect how much energy the cladding absorbs during the laser cladding process. When other process parameters remain unchanged, increasing the laser power or reducing the powder delivery rate increases the laser energy absorbed per unit mass of the cladding, reducing the cracking tendency. Conversely, increasing the cladding speed decreases the laser energy absorbed per unit mass, increasing the cracking tendency.

Guangtai Zhang et al. [12] reported the effect of laser energy density on the crack sensitivity of T-800 laser cladding coating. They found that reducing the difference between the laser cladding temperature and the initial temperature reduces the thermal stress at the interface, which leads to a decrease in cracking sensitivity. Bowen Shi et al. [13] optimally selected laser cladding parameters to prepare a Ni60A coating without cracks. The results show that higher line energy and lower powder feed can help prevent cracks but can lead to lower microhardness. To obtain a crack-free Ni60A coating with high microhardness, a combination method of preheating to 300 °C was used, which not only ensured a reduction in thermal damage to the substrate but increased the microhardness to 510–553 HV. Yingkai Feng et al. [14] prepared an Fe₃Al/Cr₃C₂ composite coating by laser cladding and studied the mechanism of the process parameters on the coating cracks. The results show that the inappropriate content proportion of the plastic phase of Fe₂AlCr, the brittle phase of Fe₃Al, and the Cr₇C₃ in the cladding coating mainly caused the crack. With the decrease in Cr₃C₂ content and the increase in Fe₂AlCr content, the ductility of the coating also increased. Laser cladding process parameters mainly affect the dilution rate of the cladding coating and thus affect the content of Fe₂AlCr in the coating, which also affects the plasticity and crack resistance of the coating.

Laser cladding process parameters not only affect the temperature field and the existence time of the molten pool but also affect the phase composition of the coating, which will affect the cracking resistance of the layer. The optimization of laser cladding process parameters can effectively reduce or eliminate coating cracks.

3. Material heat treatment method

According to Formula (1), thermal stress can be reduced when the temperature difference before and after cladding is slight. Therefore, the temperature difference can be reduced by preheating the substrate before laser cladding to inhibit the generation of cracks. The product can be annealed to reduce residual stress. Annealing is a standard heat treatment method to reduce residual stress. Laser remelting can also be used to remove

residual stress. This method allows the laser cladding coating to be reheated using a laser without disassembling the product.

Shaik E. Hoosain et al. [15] carried out heat treatment of a titanium aluminum alloy processed by laser alloying. The heat treatment of the samples can promote the homogenization of the microstructure and reduce thermal stress. Yulei Feng et al. [16] reported a method for the preheating temperature prediction of laser cladding. In their paper, they showed that preheating can reduce the occurrence of cracks in laser cladding coatings. Zhang Guangtai et al. [17] studied the effect of substrate preheating on the crack and wear resistance of a laser cladding T-800 coating. Two different temperature test substrates, namely non-preheated (22 °C) and preheated (300 °C), were used to deposit the surface of DD5 single crystal T-800 alloy coating alloy using laser cladding technology. The experimental results showed that the preheating of the substrate reduces the degree of microstructure change in each region of the coating. This effectively reduces the internal stress of the coating caused by the different solidification rates of various casting parts, thereby preventing the coating from cracking.

The principle of preheating the substrate to reduce the cracks of the laser cladding coating is to reduce the internal stress of the coating and adjust the phase composition and microstructure. The results show that preheating can effectively improve the crack generation of laser cladding coating.

4. Increase the auxiliary physical field

In recent years, researchers have found that auxiliary fields, including mechanical vibration, the electromagnetic field, the ultrasonic field, and other auxiliary fields, can act on the molten pool and affect the heat and mass transfer of the molten pool without contact with the material, thus avoiding the contamination of the cladding coating.

Qiaofeng Bai et al. [18] pointed out that the applied energy field can improve the defects of cracks, pores, and the nonuniform microstructure of a laser cladding coating by combing the research status of applied energy field-assisted laser cladding and laser cladding posttreatment. Wang Qian et al. [19] believed that applying an electromagnetic field in the laser cladding process and using the stirring effect of electromagnetic force on the molten pool to change the mass and heat transfer process could achieve the purpose of improving the quality of the cladding coating, refining the microstructure and improving performance. Sun J Y et al.'s [20] laser cladding 316L stainless steel coating found that the electromagnetic heat effect played a role in reducing the degree of supercooling thinning solidification structure, thereby reducing the sensitivity of the cladding coating cracking.

In summary, the probability of coating cracking can be effectively reduced through the above four ways. However, the heat treatment method or increasing the external physical field requires related equipment, which will undoubtedly increase the cost of coating preparation and the complexity of the preparation process. By contrast, optimizing cladding materials composition and process parameters is a simple and effective way to reduce coating cracks.

In this paper, based on optimizing the cladding parameters of A100 ultrahigh strength steel [21], different proportions of Ni and Ti elements were added to the powder, leading to the preparation of crack-free A100-(Ni-Ti) claddings coatings. The phase composition, microstructure, microhardness, and wear resistance of A100-(Ni-Ti) cladding coating were studied in this work. At the same time, the influence mechanism of Ni and Ti content on the microstructure and mechanical properties of the cladding coating was also studied.

2. Materials and Methods

Low-carbon steel was selected as the substrate of laser cladding. The low carbon steel was a hot rolled sheet produced by Guangxi Liuzhou Iron and Steel Group Co., Ltd.

(Liuzhou, China). Before laser cladding, the surface of the substrate was polished and treated to avoid rust and oil on the surface of the substrate. A100 ultra-high strength steel powders were used for laser cladding base materials. The powder morphology of A100 ultra-high strength steel is shown in Figure 1. The A100 ultra-high strength steel powder was spherical or quasi-spherical, and the powder size was generally about 60 μm . The A100 ultra-high strength steel powders were manufactured by AVIC Mette Additive Technology (Beijing) Co., Ltd. (Beijing, China). An EDS energy spectrum test was conducted on the element composition of A100 ultra-high strength steel powder (tested twice), and the test results are shown in Table 1.

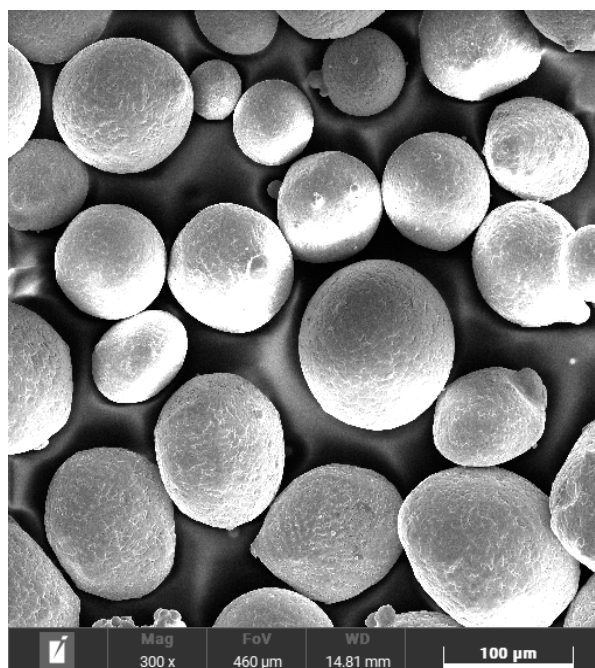


Figure 1. A100 steel powder morphology and size.

Table 1. Element composition of A100 steel powder (wt%) [21].

Elements	Fe	Co	Ni	Cr	Mo
1	69.7	14.4	11.3	3.1	1.6
2	70.5	14.6	10.9	3.3	0.8

The laser cladding process was selected with a laser power of 2000 W, a scanning speed of 6 mm/s, and a spot diameter of 4 mm. In order to improve the plastic toughness of the laser cladding samples, Ni powder and Ti powder were selected to be added to the A100 ultra-high strength steel powder according to the molar ratio of 1:1, and the addition amounts were 10 wt%, 20 wt%, and 30 wt%, respectively. The morphology of the laser cladding Ni powder and Ti powder is shown in Figure 2. In order to protect the laser cladding coating from oxidation by air, the laser cladding experiment was performed in a self-made, semi-closed box. The dimensions of the box are 20 cm, 15 cm, and 8 cm, respectively. The protective gas argon must first be filled into the box before the experiment. The influx velocity of argon was 15 L/min, and the argon gas continued to influx for 3 min.

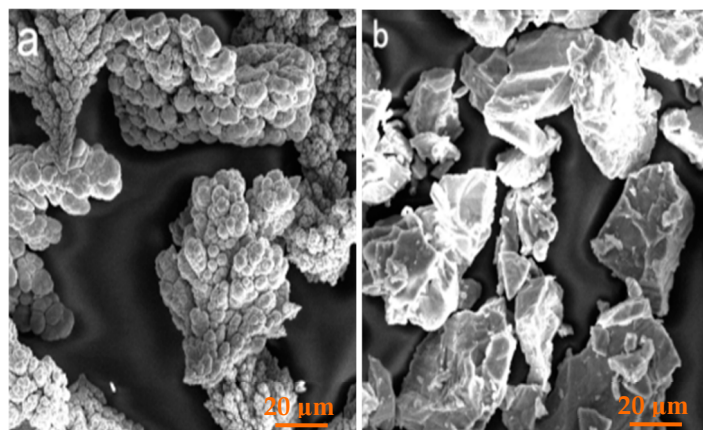


Figure 2. Laser cladding Ni and Ti powder morphologies. (a) Ni powder, (b) is Ti powder.

The phase constituents of the laser cladding coatings were analyzed by XRD (produced by Panalytical, Almelo, The Netherlands). Before XRD testing, the top surface needed to be ground with metallographic sandpaper, and then the surface was polished. The polished cladding coating was cleaned with anhydrous ethanol and then was dried as the sample to be tested by XRD. The tube voltage used in the test was 40 kV, the tube current was 40 mA, the minimum irradiation diameter of the test focal spot was 20 μm , the scanning mode was continuous scanning, the scanning angle was $2\theta = 20\text{--}90^\circ$, and the scanning rate was $5^\circ/\text{min}$. The microstructure of the cladding coatings was observed using scanning electron microscopy (SEM). Bruker Quantax 400 (Billerica, MA, USA) and a Quantax FlatQUAD energy dispersive spectrometer (EDS, San Marcos, CA, USA) were used to analyze and test the composition and distribution of the chemical elements in the selected microzone and the selected route of the cladding coating.

The cross-section of the laser cladding coating needed to be inlaid to prepare for subsequent grinding and polishing. The embedded sample was polished with metallographic sandpaper and polished with a polishing machine. The polished sample tested the microhardness distribution across the cladding coatings. An HXS-1000 type digital liquid crystal intelligent microhardness tester produced by Shanghai Hao Microlight Technology Co., Ltd. (Shanghai, China) was utilized to test the microhardness of the cladding coating. The microhardness test of the cladding coating was carried out in a straight line from the top of the coating to the substrate. The loading load was 100 g, and the pressure holding time was 15 s.

The friction and wear test of the cladding coating adopted bearing steel as the friction pair material. The friction block was the cladding samples which measured 1 cm^3 . The developed ring block friction and wear testing machine tested the tribological properties, as shown in Figure 3. The friction ring was made of bearing steel, whose chemical composition was 0.95%~1.05% C, 0.25%~0.45% Mn, 1.40%~1.65% Cr, 0.15%~0.35% Si, $\leq 0.025\%$ P, $\leq 0.025\%$ S, with the balance being iron. The microhardness of the bearing steel was about 751 HV. After the ring block friction pair was installed, the speed of the testing machine was controlled at 100 r/min, the applied load was controlled at 10 N, and the friction and wear time was 300 s. Upon completion of the friction and wear test, the mass of the friction samples before and after the test was measured using an analytical balance, and the wear loss was calculated. The balance was an electronic analytical balance produced by Shanghai Precision Instrument Co., Ltd. (Shanghai, China), with a weighing range of 0–100 g and a reading accuracy of 0.1 mg. SEM observed the microtopography of the friction surface.

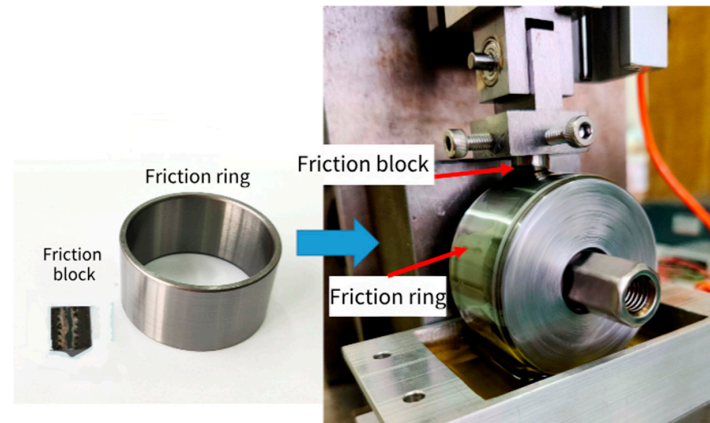


Figure 3. Friction (block) specimen and test equipment.

3. Results and Discussion

3.1. Macroscopic Morphologies of A100-(Ni-Ti) Coatings

The surface morphologies of the A100-(Ni-Ti) cladding coatings are shown in Figure 4. The surface of A100-(Ni-Ti) cladding coatings was formed continuously and has a favorable forming quality without obvious cracks and other defects.

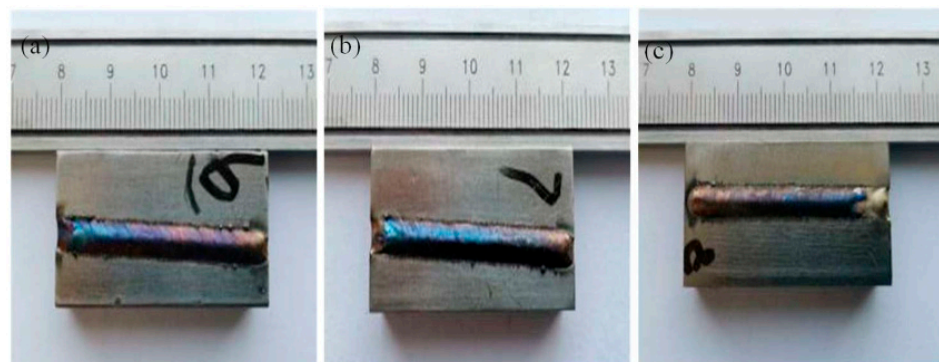


Figure 4. Surface morphologies of A100-(Ni-Ti) cladding coatings. (a) A100-10% (Ni-Ti) cladding coating surface morphology, (b) A100-20% (Ni-Ti) cladding coating surface morphology, and (c) A100-30% (Ni-Ti) cladding coating surface morphology.

The cross-section morphologies of A100-(Ni-Ti) cladding coatings are exhibited in Figure 5. The A100-(Ni-Ti) cladding coating is well combined with the matrix, and no cracks or other defects are found at the bonding interface. The crescent shape of the cladding coating is related to the Gaussian energy distribution of the circular laser spot.

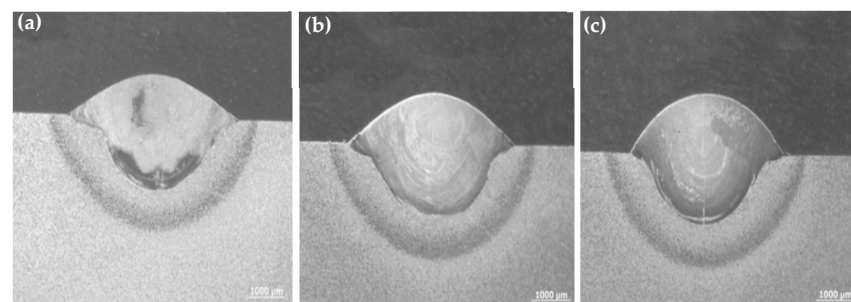


Figure 5. The cross-section morphologies of A100-(Ni-Ti) cladding coatings. (a) The A100-10%(Ni-Ti) cladding coating cross-section morphology, (b) the A100-20%(Ni-Ti) cladding coating cross-section morphology, and (c) the A100-30%(Ni-Ti) cladding coating cross-section morphology.

3.2. Phase Composition and Microstructure of A100-(Ni-Ti) Coatings

The phase composition results of A100-(Ni-Ti) cladding coatings are shown in Figure 6. It can be seen from the figure that the phases of the A100-(Ni-Ti) cladding coating mainly consist of martensite and austenite. The amount of Ni-Ti powder added does not change the main phase composition of the A100-(Ni-Ti) cladding coating. Compared with the coating without Ni-Ti, the S3 coating of the previous research [21], the main phase composition of the A100-(Ni-Ti) cladding coating did not change significantly. In addition, the diffraction peak of Fe_3O_4 is found in the XRD results, but the intensity of the diffraction peak is very low. This is due to the slight oxidation of the cladding coating in the laser cladding process, although there is argon gas protection.

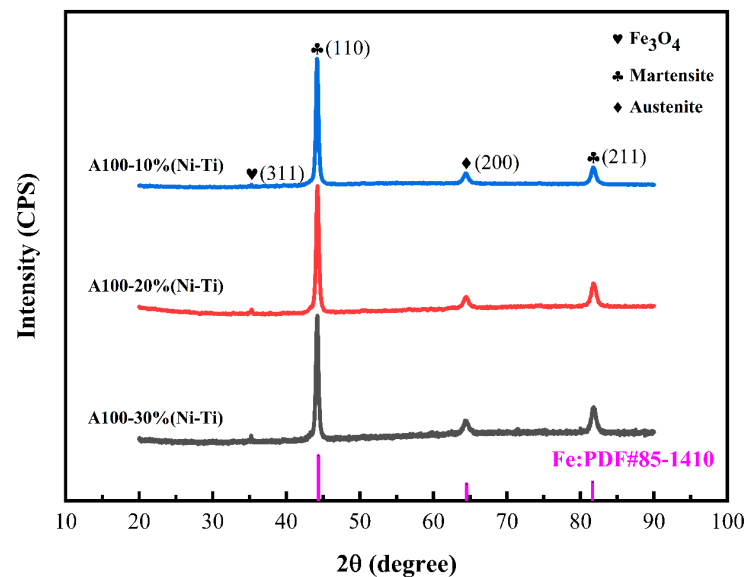


Figure 6. Phase composition results of A100-(Ni-Ti) cladding coatings.

The microstructure of the A100-(Ni-Ti) cladding coating with different Ni-Ti content is shown in Figure 7. It can be seen from Figure 7 that the microstructure of the A100-(Ni-Ti) cladding coating is mainly composed of matrix and dendrite. The grain in the lower coating is the largest within the same coating, and the grains at the top of the coating are the smallest. This is because the solidification of the molten pool starts from the lower part of the coating when the temperature gradient in the molten pool is the largest, the solidification rate is the smallest, and the grains have enough time to grow after nucleation. Compared with the upper grain of the coating, the middle grain of the coating becomes coarser. When the middle of the coating is solidified, the heat can only be transferred through the lower part of the coating that has been solidified. The heat dissipation direction is single, and the heat dissipation rate is slow, so the grain has more than enough time to grow. The grains at the top of the A100-(Ni-Ti) coating are very small because when the molten pool is solidified, the heat can dissipate to the solidified coating and the air. Therefore, the molten pool solidifies rapidly. There is not enough time for grain development after nucleation, so the grains are tiny. With the increase in Ni-Ti addition, the grains in the coating become coarser, obviously. The microstructure of the A100 coating with Ni-Ti is different from that without Ni-Ti. The microstructure of the A100 coating with Ni-Ti comprises a secondary phase and a substrate, while the A100 coating without Ni-Ti has no obvious secondary phase.

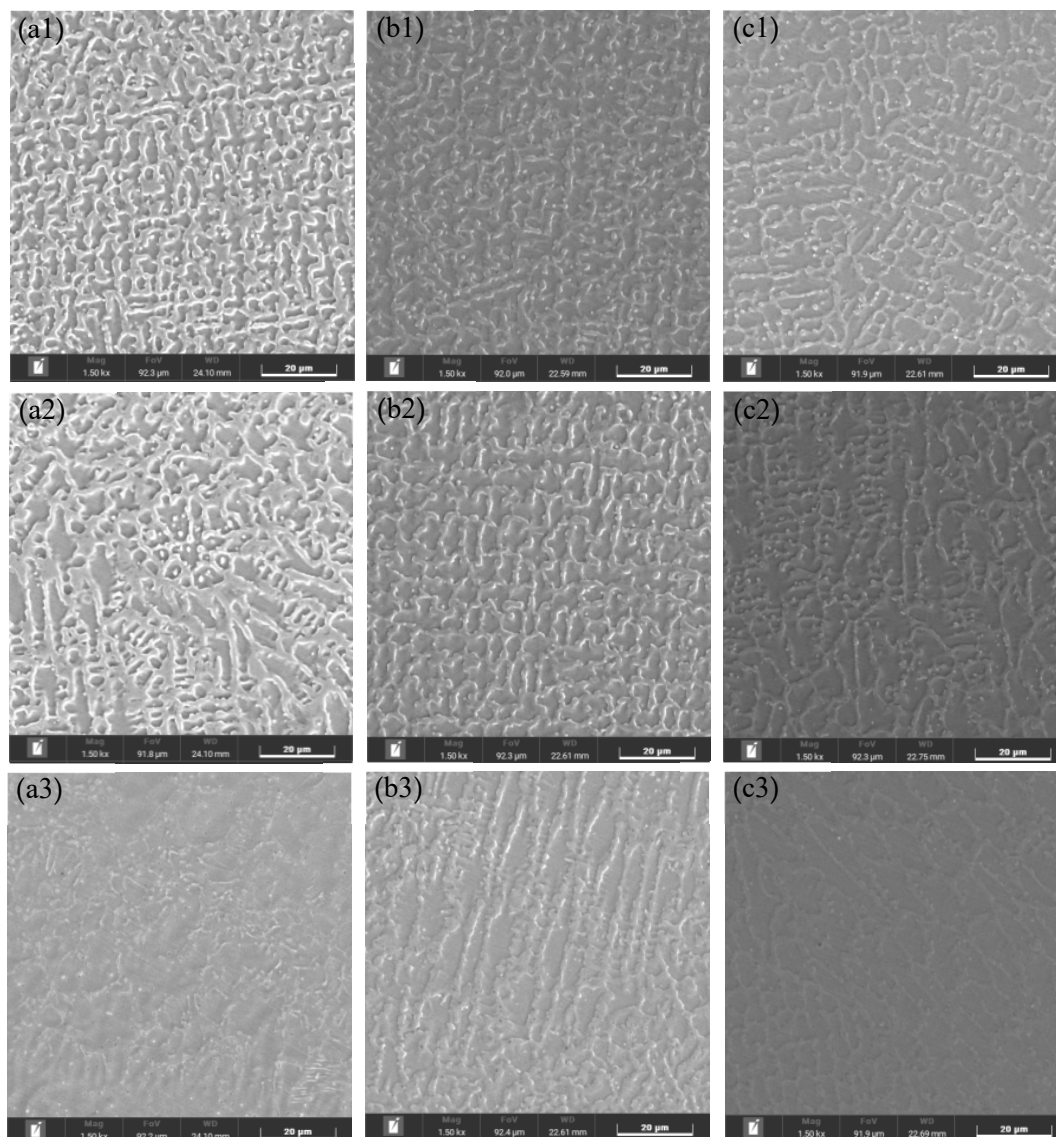


Figure 7. Microstructure of A100-(Ni-Ti) cladding coating with different (Ni-Ti) contents. **(a1)** A100-10%(Ni-Ti) cladding coating upper, **(a2)** A100-10%(Ni-Ti) cladding coating middle, **(a3)** A100-10%(Ni-Ti) cladding coating lower, **(b1)** A100-20%(Ni-Ti) cladding coating upper, **(b2)** A100-20%(Ni-Ti) cladding coating middle, **(b3)** A100-20%(Ni-Ti) coating lower, **(c1)** A100-30%(Ni-Ti) coating upper, **(c2)** A100-30%(Ni-Ti) coating middle, and **(c3)** A100-30%(Ni-Ti) coating lower.

In order to analyze the distribution of the alloying elements, EDS surface scanning analysis of elements was performed on the high-power microstructure of the middle of the A100-20%(Ni-Ti) cladding coating, and the results are shown in Figure 8. It can be seen from the figure that Ni elements are mainly concentrated in the dark gray irregular polygon secondary phase, and the distribution of Fe, Co, and Mo elements is relatively uniform, and there is no apparent aggregation. According to the phase analysis results of the A100-(Ni-Ti) coating, the secondary phase of the dark gray irregular polygon (orange dotted line area) is austenite, and the coating matrix is martensite (blue dotted line area).

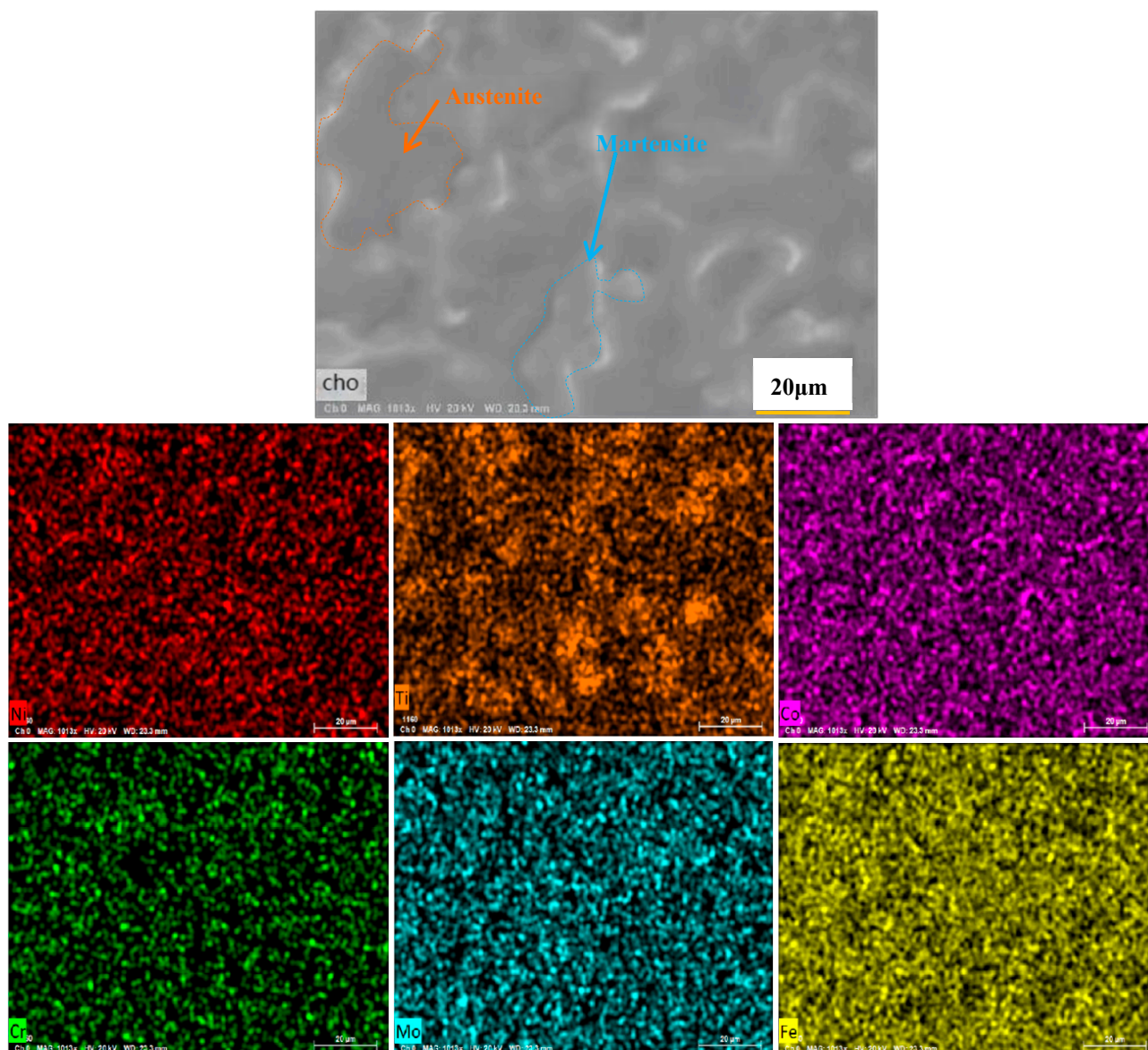


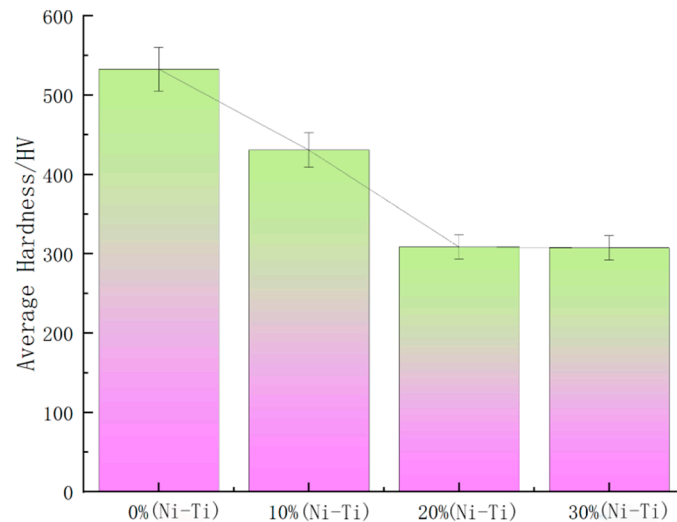
Figure 8. EDS surface scanning analysis of the middle part of the A100-20%(Ni-Ti) cladding coating.

3.3. Microhardness and Wear Resistance of A100-(Ni-Ti) Coatings

The microhardness test was performed three times for each coating, the maximum and minimum values of the test results were recorded, and the average value of the test results was calculated. The microhardness values of A100-(Ni-Ti) cladding coatings are shown in Table 2. It can be seen from Table 1 that with the increase in Ni-Ti addition, the average value of the microhardness test of the coating gradually decreases. In order to visually compare the microhardness of the A100 coating with Ni-Ti and without Ni-Ti, Figure 9 displays the microhardness of A100-(Ni-Ti) cladding coatings. As can be seen from Figure 9, the microhardness of cladding coatings decreased significantly compared with the A100 cladding without Ni-Ti (i.e., S3 coating [21]). After the addition of Ni-Ti, the austenite content of the A100 coating is increased, and the hardness is lower than that of martensite austenite, so the microhardness of the coating is reduced.

Table 2. Microhardness values of A100-(Ni-Ti) cladding coatings.

Coating Samples	Maximum Values (HV)	Minimum Values (HV)	Average Value (HV)
A100-10%(Ni-Ti)	479.51	374.71	430.99
A100-20%(Ni-Ti)	335.33	274.23	308.64
A100-30%(Ni-Ti)	332.62	284.87	307.49

**Figure 9.** Microhardness of A100-(Ni-Ti) cladding coatings.

The morphologies of the friction and wear surface of A100-(Ni-Ti) cladding coatings are shown in Figure 10. It can be intuitively seen from the figure that there are a small number of pitting pits and adhesive wear pits on the wear surface of the A100-10%(Ni-Ti) cladding coating. When Ni-Ti is 20% and 30%, the coating wear is severe, manifested as significant adhesive wear. The wear surface of the A100-0%(Ni-Ti) coating (i.e., the S3 coating [21]) has an obvious adhesive wear pit. The microhardness of the A100-10%(Ni-Ti) coating is lower than that of the A100-0%(Ni-Ti) coating. However, the surface wear degree of the A100-10%(Ni-Ti) coating is not as severe as that of the A100-0%(Ni-Ti) coating. The bearing steel friction ring forms a friction pair with the surface of the cladding coating. The friction between the friction pairs is formed by the friction ring squeezing the surface of the cladding coating. In the process of friction and wear, the friction heat between the friction pairs causes the surface material of the cladding coating to plasticize. Under friction, the plasticized material on the surface of the cladding coating will glue with the friction ring. Due to the relative motion between the friction pairs, the plasticized material on the surface of the cladding coating is torn by the friction ring and peeled off, thus forming an adhesive wear pit on the wear surface of the cladding coating. When the microhardness of the cladding coating is moderate, on the one hand, the hardness is too low, and it is easy to glue with the friction ring to cause material stripping; on the other hand, the surface material of the cladding coating can reduce friction and wear through elastic deformation and good coordination with the friction ring, so that the cladding coating shows ideal frictional conformability [22]. Nevertheless, when the amount of Ni-Ti is increased by 20% and 30%, the microhardness of the cladding coating decreases significantly, leading to severe adhesive wear.

The wear loss of the A100-(Ni-Ti) cladding coating is shown in Figure 11. It can be seen from the figure that the wear loss of the A100-10%(Ni-Ti) cladding coating is the least. Due to the highest microhardness, the wear loss of the cladding coating without Ni-Ti is not much different from that of the A100-10%(Ni-Ti) cladding coating. When the additive

amount of Ni-Ti is 20% and 30%, the microhardness and wear resistance of the cladding coatings are significantly reduced, and the surface materials of the coatings are peeled off due to wear, so the wear loss is increased considerably.

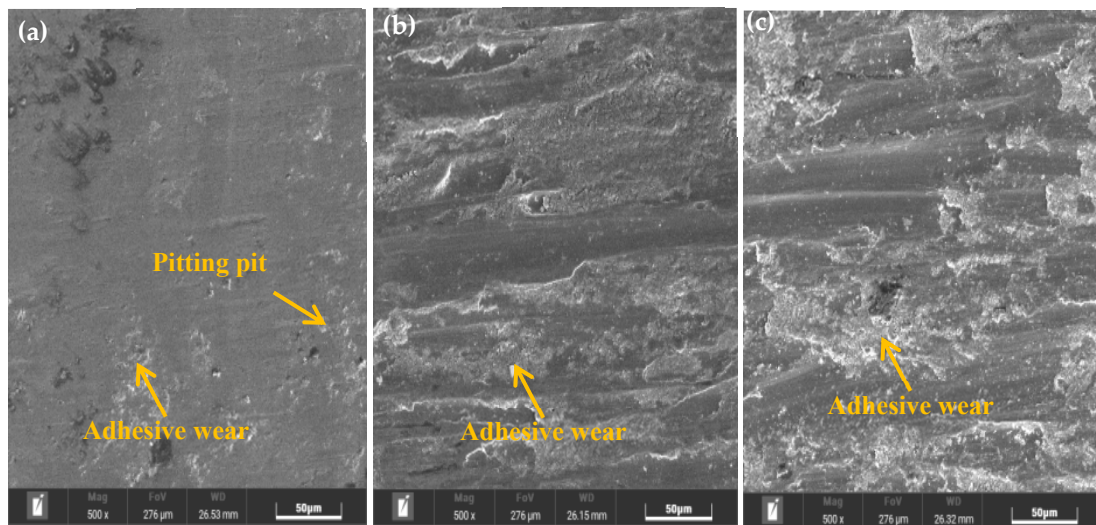


Figure 10. Friction–wear surface morphologies of A100-(Ni-Ti) cladding coatings. (a) A100-10%(Ni-Ti) cladding coating, (b) A100-20%(Ni-Ti) cladding coating, and (c) A100-30%(Ni-Ti) cladding coating.

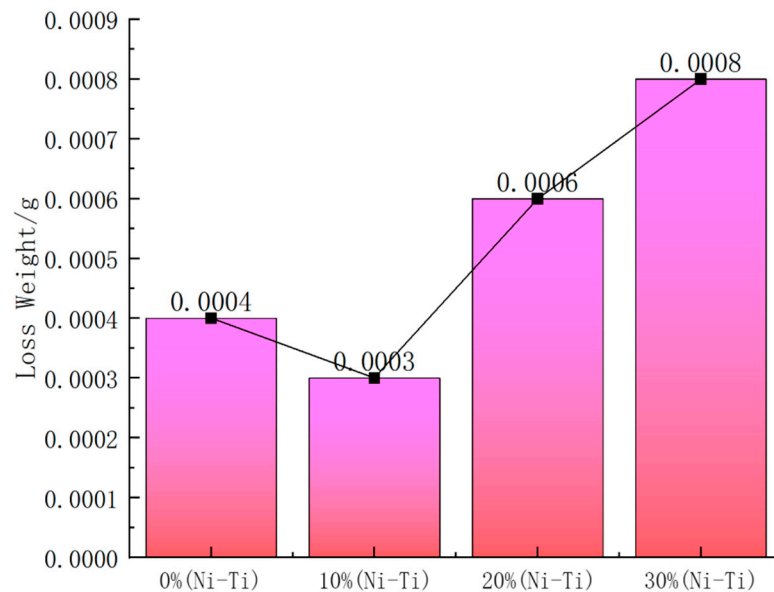


Figure 11. Loss of wear of A100-(Ni-Ti) cladding coatings.

4. Conclusions

1. To improve the plastic toughness and crack resistance of A100 laser cladding coatings, A100-(Ni-Ti) cladding coatings without cracks were manufactured by laser cladding technology by adding Ni and Ti powders of equal molar ratio as raw cladding materials. The effects of Ni-Ti addition on the microstructure, microhardness, and wear resistance of the A100 cladding coating and the following conclusions were studied.

A100-(Ni-Ti) cladding coatings mainly contain martensite and austenite. The added Ni and Ti elements are distributed primarily in the austenite region. In the cladding coatings, the upper part of the coating is relatively fine dendrites or equiaxed grains, while the grains in the lower part of the coating are coarse columnar grains. With the increase in Ni and Ti elements, the microstructure of the cladding coating gradually becomes coarse.

2. The microhardness of the A100 cladding coating without Ni and Ti is 532.50 HV. After adding Ni and Ti elements, the microhardness of A100 cladding coatings decreases significantly. The microhardness of A100-30%(Ni-Ti) cladding coating is only 307.49 HV. After adding Ni and Ti elements, the microhardness of the cladding coating decreases significantly.
3. The wear surface of the A100-10%(Ni-Ti) cladding coating contains mainly pits and a small amount of adhesive wear. A100-20%(Ni-Ti) and A100-30%(Ni-Ti) cladding coatings show severe adhesive wear. The A100-10%(Ni-Ti) cladding coating has the smallest wear loss of 0.0003 g. The A100-10%(Ni-Ti) cladding coating has relatively high microhardness and good run-in performance, with the best wear resistance.

Author Contributions: Conceptualization, T.H.; Methodology, X.Z.; Software, X.M.; Validation, X.Y. and B.W.; Formal analysis, B.W. and T.Y.; Investigation, X.M.; Resources, T.H.; Data curation, P.L.; Writing—original draft, X.Y.; Writing—review & editing, X.Z. All authors have read and agreed to the published version of the manuscript.

Funding: This work was funded by the Jiangsu Province Industrial Sensing and Intelligent Manufacturing Equipment Engineering Research Center Open Fund Project #1 under grant number 201050622ZK002; the project of the Talent Introduction and Scientific Research Start-Up Fund of Nanjing Vocational University of Industry Technology #2 under grant number YK21-01-05; and the Open Foundation of Industrial Perception and Intelligent Manufacturing Equipment Engineering Research Center of Jiangsu Province #3.

Institutional Review Board Statement: Not applicable.

Informed Consent Statement: Not applicable.

Data Availability Statement: Data are contained within the article.

Conflicts of Interest: The authors declare no conflicts of interest.

References

1. Qiu, B.; Jia, L.; Yang, H.; Guo, Z.; Jiang, C.; Li, S.; Sun, B. Study on the Effect of Pressure on the Microstructure, Mechanical Properties, and Impact Wear Behavior of Mn-Cr-Ni-Mo Alloyed Steel Fabricated by Squeeze Casting. *Metals* **2024**, *14*, 1054. [[CrossRef](#)]
2. Han, T.; Zhou, K.; Chen, Z.; Gao, Y. Research Progress on Laser Cladding Alloying and Composite Processing of Steel Materials. *Metals* **2024**, *12*, 2055. [[CrossRef](#)]
3. Han, Y.; Fu, H. Improvement of High Temperature Wear Resistance of Laser-Cladding High-Entropy Alloy Coatings: A Review. *Metals* **2024**, *14*, 1065. [[CrossRef](#)]
4. Zhan, D.; Jiang, D.; Tong, Y.; Zhang, M.; Zhang, J.; Hu, H.; Zhang, Z.; Wang, K. Effect of Electromagnetic Field Assistance on the Wear and Corrosion Resistance of Nickel-Based Coating by Laser Cladding. *Metals* **2024**, *14*, 998. [[CrossRef](#)]
5. Han, T.; Xiao, M.; Zhang, J. Laser cladding composite coating on mild steel using Ni-Cr-Ti-B₄C powder. *Surf. Eng.* **2020**, *36*, 1278–1284. [[CrossRef](#)]
6. Yang, P.; Lu, N.; Liang, J.; Guo, Y.; Zhang, G.; Song, X.; Zhou, Y.; Sun, X.; Li, J. Hot Crack Formation Mechanism and Inhibition of a Novel Cobalt-Based Alloy Coating During Laser Cladding. *Materials* **2024**, *17*, 3914. [[CrossRef](#)] [[PubMed](#)]
7. Tan, Q.; Liu, K.; Li, J.; Geng, S.; Sun, Y.; Skuratov, V. A review on cracking mechanism and suppression strategy of nickel-based superalloys during laser cladding. *J. Alloys Compd.* **2024**, *1001*, 175164. [[CrossRef](#)]
8. Hou, S.; Ren, C.; Wu, C.; Zhao, J.; Zhang, D.; Zhang, H. A Review of Crack Generation and Suppression in Laser Cladding Layer. *Mater. Rep.* **2021**, *35*, 352–356.
9. Shen, X.; He, X.; Gao, L.; Su, G.; Xu, C.; Xu, N. Study on crack behavior of laser cladding ceramic-metal composite coating with high content of WC. *Ceram. Int.* **2022**, *48*, 17460–17470. [[CrossRef](#)]
10. Li, Z.; Lin, T.; Jing, C.; Tu, Y.; Fu, T.; Liu, N. Influence of Ti element on the microstructure and crack of modulated WC-strengthened Ni-based alloy coatings by laser cladding. *Mater. Today Commun.* **2024**, *41*, 110541. [[CrossRef](#)]
11. Li, M.; Zhang, J.; Mi, T.; Zheng, C.; Wu, D.; Chen, Z.; Yi, X. Improvement mechanism of Mo element on cracks, microstructure and properties of laser cladding WC-Ni60AA coating. *Surf. Coat. Technol.* **2024**, *489*, 131047. [[CrossRef](#)]

12. Zhang, G.; Liu, W.; Bian, H.; Wang, H.; Wang, W.; Xu, X.; Liu, J. Effect of laser energy density on cracking susceptibility and wear resistance of laser-clad triballoy T-800 coatings on DD5 single-crystal alloys. *Mater. Today Commun.* **2024**, *40*, 109604. [[CrossRef](#)]
13. Shi, B.; Li, T.; Guo, Z.; Zhang, X.; Zhang, H. Selecting process parameters of crack-free Ni60A alloy coating prepared by coaxial laser cladding. *Opt. Laser Technol.* **2022**, *149*, 107805. [[CrossRef](#)]
14. Feng, Y.; Liu, S.; Zhao, J.; Zhao, L.; Liu, Z. Influential Mechanism of Cr₃C₂ Content and Process Parameters on Crack Generation of Fe₃Al/Cr₃C₂ Composites. *Coatings* **2023**, *13*, 1636. [[CrossRef](#)]
15. Hoosain, S.E.; Pityana, S.; Freemantle, C.S.; Tlotleng, M. Heat Treatment of In Situ Laser-Fabricated Titanium Aluminide. *Metals* **2018**, *8*, 655. [[CrossRef](#)]
16. Feng, Y.; Pang, X.; Feng, K.; Feng, Y.; Li, Z. A method for evaluating the crack resistance and predicting the preheating temperature of high hardness coating prepared by laser cladding. *Surf. Coat. Technol.* **2022**, *432*, 128076. [[CrossRef](#)]
17. Zhang, G.; Liu, W.; Bian, H.; Xing, F.; Xu, X. Effect of Substrate Preheating on Cracking and Wear Resistance of Laser-Cladded Triballoy T-800 Coatings on DD5 Single-Crystal Alloy. *J. Therm. Spray Technol.* **2024**, *33*, 1027–1039. [[CrossRef](#)]
18. Bai, Q.; Chen, C.; Li, Q.; Zhao, C. Status of Research on Assisted Laser Cladding and Laser Cladding Posttreatment: A Review. *Phys. Met. Metallogr.* **2024**. [[CrossRef](#)]
19. Qian, W.; Liang, Z.; Qian, L.; Zhang, J.; Ban, C. Research Progress of Electromagnetic Field Assisted Laser Cladding Technology. *Surf. Technol.* **2023**, *52*, 166–179. [[CrossRef](#)]
20. Sun, J.; Yu, Z.; Lin, Y.; Zhao, X.; Qu, W.; Yu, T. Effect of shielding gas flow rate on cladding quality of direct laser fabrication AISI 316L stainless steel. *J. Manuf. Process.* **2019**, *48*, 51–65. [[CrossRef](#)]
21. Han, T.; Ding, Z.; Feng, W.; Yao, X.; Chen, F.; Gao, Y. Effects of Process Parameters on Microstructure and Wear Resistance of Laser Cladding A-100 Ultra-High-Strength Steel Coatings. *Coatings* **2024**, *14*, 669. [[CrossRef](#)]
22. Mao, J.; Chen, G.; Zhao, J.; He, Y.; Luo, J. An investigation on the tribological behaviors of steel/copper and steel/steel friction pairs via lubrication with a graphene additive. *Friction* **2021**, *9*, 228–238. [[CrossRef](#)]

Disclaimer/Publisher's Note: The statements, opinions and data contained in all publications are solely those of the individual author(s) and contributor(s) and not of MDPI and/or the editor(s). MDPI and/or the editor(s) disclaim responsibility for any injury to people or property resulting from any ideas, methods, instructions or products referred to in the content.